

## Charge dependence of the nucleon-nucleon interaction

G. Q. Li\* and R. Machleidt†

Department of Physics, University of Idaho, Moscow, Idaho 83844

(Received 29 July 1998)

Based upon the Bonn meson-exchange-model for the nucleon-nucleon ( $NN$ ) interaction, we calculate the charge-independence breaking (CIB) of the  $NN$  interaction due to pion-mass splitting. Besides the one-pion exchange (OPE), we take into account the  $2\pi$ -exchange model and contributions from three and four irreducible pion exchanges. We calculate the CIB differences in the  $^1S_0$  effective range parameters as well as phase-shift differences for partial waves up to total angular momentum  $J=4$  and laboratory energies below 300 MeV. We find that the CIB effect from OPE dominates in all partial waves. However, the CIB effects from the  $2\pi$  model are noticeable up to  $D$  waves and amount to about 40% of the OPE CIB contribution in some partial waves, at 300 MeV. The effects from  $3\pi$  and  $4\pi$  contributions are negligible except in  $^1S_0$  and  $^3P_2$ . [S0556-2813(98)03112-4]

PACS number(s): 24.80.+y, 11.30.Hv, 13.75.Cs, 21.30.Cb

### I. INTRODUCTION

It is well known that isospin invariance is not an exact symmetry of strong interactions. Consequently, nuclear forces have a small but measurable charge-dependent component. The equality between proton-proton ( $pp$ ) [or neutron-neutron ( $nn$ )] and neutron-proton ( $np$ ) nuclear interactions is known as charge independence. Charge-independence breaking (CIB) is seen most clearly in the  $^1S_0$  nucleon-nucleon ( $NN$ ) scattering lengths. The latest empirical values for the singlet scattering length  $a$  and effective range  $r$  are [1]

$$\begin{aligned} a_{pp}^N &= -17.3 \pm 0.4 \text{ fm}, & r_{pp}^N &= 2.85 \pm 0.04 \text{ fm}, \\ a_{nn}^N &= -18.8 \pm 0.3 \text{ fm}, & r_{nn}^N &= 2.75 \pm 0.11, \end{aligned} \quad (1)$$

$$a_{np} = -23.75 \pm 0.01 \text{ fm}, \quad r_{np} = 2.75 \pm 0.05 \text{ fm}.$$

The values given for  $pp$  and  $nn$  scattering refer to the nuclear part of the interaction as indicated by the superscript  $N$ . Electromagnetic effects have been removed from the experimental values, which is model dependent. The uncertainties quoted for  $a_{pp}^N$  and  $r_{pp}^N$  are mainly due to this model dependence.

It is useful to define the following averages:

$$\bar{a} \equiv \frac{1}{2}(a_{pp}^N + a_{nn}^N) = -18.05 \pm 0.5 \text{ fm}, \quad (2)$$

$$\bar{r} \equiv \frac{1}{2}(r_{pp}^N + r_{nn}^N) = 2.80 \pm 0.12 \text{ fm}. \quad (3)$$

By definition, CIB is the difference between the  $np$  values and these averages:

$$\Delta a_{\text{CIB}} \equiv \bar{a} - a_{np} = 5.7 \pm 0.5 \text{ fm}, \quad (4)$$

$$\Delta r_{\text{CIB}} \equiv \bar{r} - r_{np} = 0.05 \pm 0.13 \text{ fm}. \quad (5)$$

Thus, the  $NN$  singlet scattering length shows a clear signature of CIB in strong interactions.

Charge dependence of  $NN$  interactions has been the subject of extensive investigations, both experimentally and theoretically, for many decades (for recent reviews, see Refs. [1,2]). The current understanding is that the charge dependence of nuclear forces is due to differences in the up and down quark masses and electromagnetic interactions. On a more phenomenological level, major causes of CIB are (i) mass splitting of isovector mesons; particularly,  $\pi$  and  $\rho$ ; (ii) irreducible pion-photon exchanges.

It has been known for a long time that the difference between the charged and neutral pion masses in the one-pion-exchange (OPE) potential accounts for about 50% of  $\Delta a_{\text{CIB}}$ . In Ref. [3], charge-dependent interactions were derived for  $np$  and  $pp$  scattering, based on a preliminary version of the Bonn meson-exchange model [4] taking into account the pion mass difference in OPE as well as two-boson exchanges. With these interactions, about 80% of the empirical  $\Delta a_{\text{CIB}}$  could be explained. Earlier, Ericson and Miller [5] had obtained a very similar result using the meson-exchange model of Partovi and Lomon [6].

The calculations of Refs. [3,5] were performed only for the singlet scattering length. However, it is also of interest to know the charge-dependent effects for intermediate energies and in partial waves other than  $^1S_0$ . Therefore, it is the main purpose of the present investigation to calculate phase-shift differences between  $pp$  (or  $nn$ ) and  $np$  scattering for states with total angular momentum  $J \leq 4$  and laboratory incident kinetic energies  $T_{\text{lab}} \leq 300$  MeV. This paper complements an earlier one on charge asymmetry of the  $NN$  interaction [7].

In Sec. II, we will discuss various classes of irreducible meson-exchange diagrams and calculate their CIB effects—due to pion-mass splitting—on  $NN$  phase shifts and singlet effective range parameters. Summary and conclusions are given in Sec. III.

\*Present address: Department of Physics, SUNY, Stony Brook, NY 11794.

†Electronic address: machleid@uidaho.edu

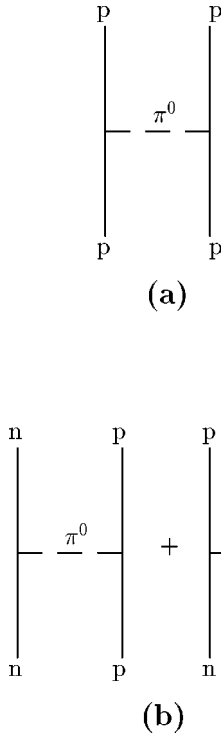


FIG. 1. One-pion-exchange (OPE) contribution to (a)  $pp$  and (b)  $np$  scattering.

## II. THE BONN MODEL AND CHARGE DEPENDENCE

The Bonn meson-exchange model for the  $NN$  interaction has been described in detail in the literature [8–10]. It is a field-theoretic model that, apart from the well-known one-boson-exchange terms, includes an explicit model for the  $2\pi$  exchange,  $\pi\rho$  diagrams, and some further contributions of  $3\pi$  and  $4\pi$  exchange. The Bonn model yields an excellent description of the  $NN$  scattering data below pion production threshold [10] and, thus, provides a reliable basis for an investigation of the charge dependence of the  $NN$  interaction. Within the model, charge dependence is created by the mass difference between the charge states of mesons. The Bonn model includes three isovector mesons, namely,  $\pi$ ,  $\rho(770)$ , and  $a_0/\delta(980)$ . We will focus here mainly on the charge-dependent effects due to pion mass difference. Effects due to  $\rho$ -mass splitting will be discussed briefly at the end of this section, and mass splitting of the  $a_0/\delta(980)$  will be ignored since nothing is known.

We use averages for the baryon masses: the average nucleon mass  $M_N=938.919$  MeV and the average  $\Delta$  mass  $M_\Delta=1232$  MeV. The pion masses are

$$m_{\pi^\pm}=139.568 \text{ MeV}, \quad m_{\pi^0}=134.974 \text{ MeV}. \quad (6)$$

The values are based upon the 1992 Review of Particle Properties [11].

The interaction Lagrangians involving pions are

$$\mathcal{L}_{\pi NN}=\frac{f_{\pi NN}}{m_{\pi^\pm}}\bar{\psi}\gamma_\mu\gamma_5\tau\psi\cdot\partial^\mu\varphi_\pi, \quad (7)$$

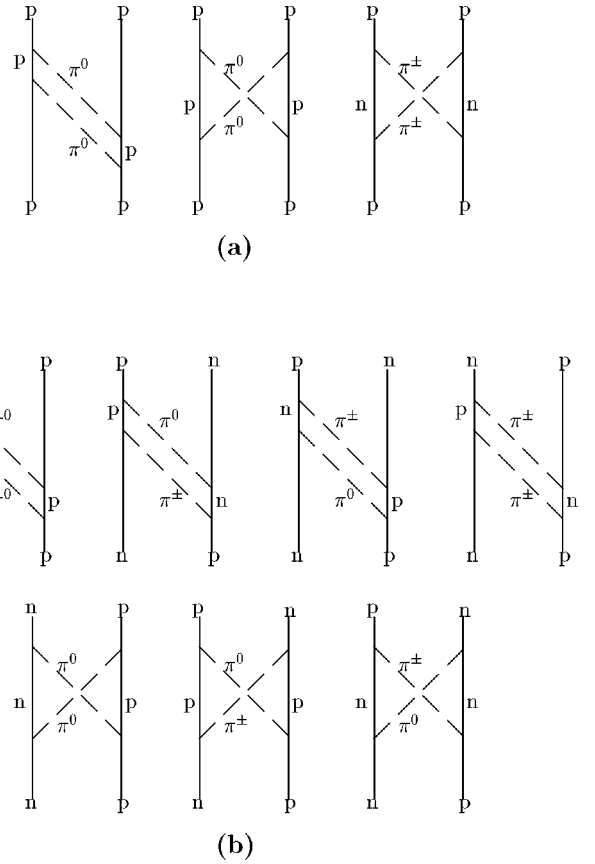


FIG. 2. Irreducible  $2\pi$ -exchange diagrams with  $NN$  intermediate states for (a)  $pp$  and (b)  $np$  scattering.

$$\mathcal{L}_{\pi N\Delta}=\frac{f_{\pi N\Delta}}{m_{\pi^\pm}}\bar{\psi}T\psi_\mu\cdot\partial^\mu\varphi_\pi+\text{H.c.}, \quad (8)$$

with  $\psi$  being the nucleon,  $\psi_\mu$  is the  $\Delta$  (Rarita-Schwinger spinor), and  $\varphi_\pi$  are the pion fields.  $\tau$  are the usual Pauli matrices describing isospin 1/2 and  $T$  is the isospin transition operator. H.c. denotes the Hermitean conjugate.

The Lagrangians are divided by  $m_{\pi^\pm}$  to make the coupling constants  $f$  dimensionless. Following established conventions [12], we always use  $m_{\pi^\pm}$  as scaling mass. It may be tempting to use  $m_{\pi^0}$  for  $\pi^0$  coupling. Notice, however, that the scaling mass could be anything. Therefore, it is reasonable to keep the scaling mass constant within SU(3) multiplets [12]. This avoids the creation of unmotivated CIB.

In our investigation of charge-dependent effects on the  $NN$  interaction, we start from a case that may be denoted the average between  $pp$  and  $nn$  scattering. For this case, our model yields  $-18.05$  fm for the singlet scattering length and  $2.864$  fm for the effective range, consistent with Eqs. (2) and (3). The one-pion-exchange contribution for this average case is depicted in Fig. 1(a) and  $2\pi$ -exchange contributions are shown in Figs. 2(a), 3(a), and 4(a). Note that, in this case, the proton  $p$  in Figs. 1(a)–4(a) carries the average nucleon mass of  $938.919$  MeV and there are no electromagnetic interactions; equally well, one may use a neutron  $n$  in place of the proton in part (a) of all figures.

To calculate the effects of charge dependence on the  $NN$  phase shifts, we introduce for each  $LSJ$  state the CIB phase shift difference  $\Delta\delta_{\text{CIB}}^{LSJ}(T_{\text{lab}})$ , defined by

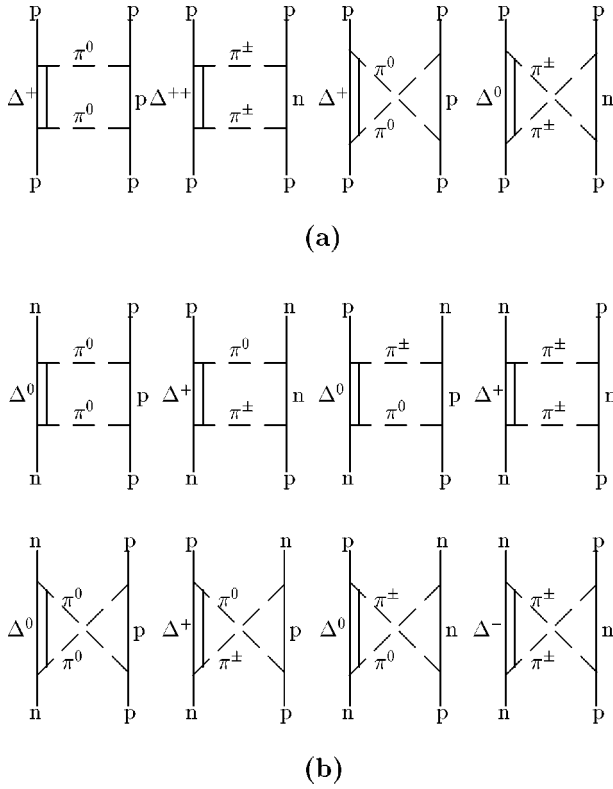


FIG. 3.  $2\pi$ -exchange contributions with  $N\Delta$  intermediate states to (a)  $pp$  and (b)  $np$  scattering.

$$\Delta \delta_{\text{CIB}}^{LSJ}(T_{\text{lab}}) \equiv \delta_{np}^{LSJ}(T_{\text{lab}}) - \bar{\delta}^{LSJ}(T_{\text{lab}}), \quad (9)$$

where  $\bar{\delta}^{LSJ}$  denotes the average of the  $pp$  and  $nn$  phase shifts which, as discussed, is calculated by taking the diagrams Figs. 1(a)–4(a) into account (besides the other diagrams involved in the Bonn model) with average nucleon mass and all electromagnetic interactions switched off. The phase shift  $\delta_{np}^{LSJ}$  is the  $np$  one to be calculated below. Similarly, we define the CIB mixing parameter difference  $\Delta \epsilon_{\text{CIB}}^J$ ,

$$\Delta \epsilon_{\text{CIB}}^J(T_{\text{lab}}) \equiv \epsilon_{np}^J(T_{\text{lab}}) - \bar{\epsilon}^J(T_{\text{lab}}). \quad (10)$$

The charge-dependence generated by the model under consideration is now “switched on” step by step:

(1) One-pion-exchange (OPE), Fig. 1: The CIB effect is created by replacing the diagram of Fig. 1(a) by the two diagrams of Fig. 1(b). Note that one-meson-exchange contributions are roughly proportional to  $1/m_\alpha^2$  (with  $m_\alpha$  the meson mass) because this is approximately the momentum-space one-meson propagator for very low momentum transfer. Thus, since the  $\pi^0$  has a smaller mass than the  $\pi^\pm$ ,  $\pi^0$  exchange is stronger than  $\pi^\pm$  exchange. For this reason, OPE is stronger in  $pp$  as compared to  $np$ . Since OPE is repulsive in  $^1S_0$ , this phase shift becomes more attractive (i. e., larger) when going from  $pp$  to  $np$ , resulting in a positive  $\Delta\delta$ ; cf. column “OPE” in Table I and dashed curve in Fig. 5. Consistent with this is the well-known fact that OPE takes care of about 50% of  $\Delta a_{\text{CIB}}$ . In the other partial waves, the sign of  $\Delta\delta$  due to OPE depends on if OPE is repulsive or attractive (e.g., it is repulsive in  $^3P_1$  and attractive in  $^3P_0$  and  $^3P_2$ ). Due to the small mass of the pion, OPE is a

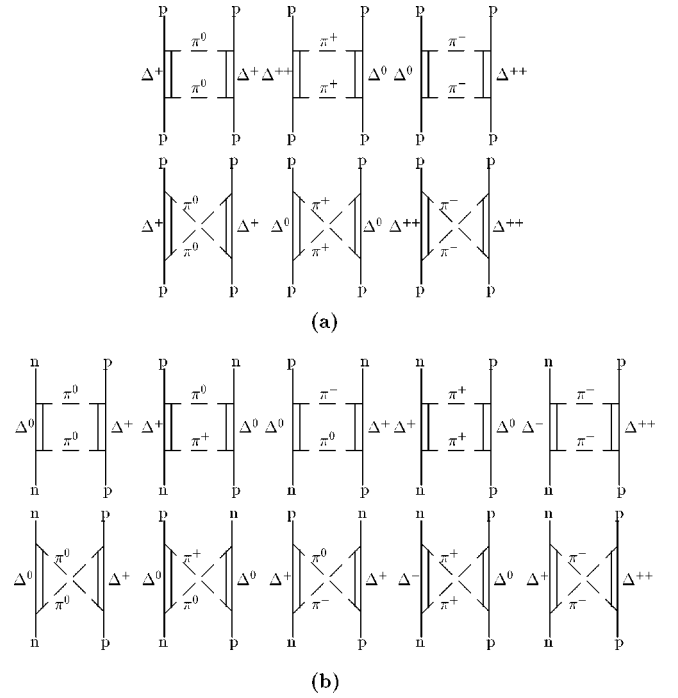


FIG. 4.  $2\pi$ -exchange contributions with  $\Delta\Delta$  intermediate states to (a)  $pp$  and (b)  $np$  scattering.

sizable contribution in all partial waves including higher partial waves; and due to the pion’s relatively large mass splitting (3.4%), OPE creates relatively large charge-dependent effects in all partial waves (Fig. 5 and Table I).

(2)  $2\pi$  exchange with  $NN$  intermediate states ( $2\pi NN$ ), Fig. 2: Notice first that only noniterative (irreducible) diagrams are to be considered, since the iterative ones are generated by the scattering equation from OPE. We mention here that, in our approach which is based upon time-ordered perturbation theory, we always take all time orderings into account (except for those that imply antibaryons in intermediate states); however, to save space, we display only a few characteristic time orderings in Fig. 2 (this is also true for all diagrams shown in Figs. 3 and 4; to get an impression of the total number of time-ordered diagrams, see Fig. 20 of Ref. [8]). The CIB effect is obtained by replacing the diagrams Fig. 2(a) ( $pp/nn$  scattering) by those of Fig. 2(b) ( $np$  scattering). For a good understanding of CIB effects, it is important to distinguish between box (here: stretched box) and crossed box diagrams. Concerning the effect from stretched box diagrams, one replaces the left diagram of Fig. 2(a) by the four stretched box diagrams of Fig. 2(b) (and similarly for the other stretched box time orderings not shown). Notice now that in the former diagram two  $\pi^0$  are exchanged making this a “strong” diagram, while the latter four diagrams together with their isospin factors result in a weaker contribution. Since  $2\pi$  exchange is, in general, attractive, there is a loss of attraction when going from  $pp$  to  $np$  (equivalent to a reduction of the phase shift). This qualitative estimate is clearly confirmed by the quantitative results displayed in column “ $2\pi NN-S$ ” of Table II. The CIB effect that stems from crossed box diagrams is obtained by replacing the two crossed boxes of Fig. 2(a) by the three crossed boxes of Fig. 2(b). Typically, this effect (column  $2\pi NN-X$  of Table II) is of opposite sign as compared to the corresponding

TABLE I. CIB phase differences (in degrees) as defined in Eqs. (9) and (10) and explained in the text.

$T_{\text{lab}}$ (MeV)	OPE	$2\pi$	$\pi\rho$	$\pi\sigma + \pi\omega$	Total	$T_{\text{lab}}$ (MeV)	OPE	$2\pi$	$\pi\rho$	$\pi\sigma + \pi\omega$	Total
			$^1S_0$			50	-0.045	0.000	0.000	0.000	-0.045
1	3.051	0.319	-0.361	1.355	4.364	100	-0.070	-0.001	0.000	0.000	-0.071
5	1.767	0.154	-0.193	0.719	2.446	150	-0.084	-0.001	0.000	0.000	-0.084
10	1.364	0.103	-0.147	0.545	1.864	200	-0.093	-0.001	0.000	0.000	-0.093
25	0.944	0.047	-0.107	0.391	1.275	300	-0.102	-0.001	-0.001	0.001	-0.102
50	0.712	0.009	-0.090	0.318	0.950						
100	0.563	-0.031	-0.083	0.276	0.725				$\epsilon_2$		
150	0.519	-0.061	-0.086	0.267	0.638	5	0.012	0.000	0.000	0.000	0.012
200	0.509	-0.091	-0.093	0.269	0.595	10	0.036	0.000	0.000	0.000	0.036
300	0.544	-0.163	-0.121	0.300	0.559	25	0.091	0.001	0.000	0.000	0.092
			$^3P_0$			50	0.119	0.002	0.000	0.001	0.121
1	-0.032	0.000	0.000	0.000	-0.032	100	0.095	0.007	-0.001	0.001	0.102
5	-0.246	-0.003	0.000	-0.001	-0.250	150	0.057	0.011	-0.002	0.002	0.068
10	-0.482	-0.009	0.001	-0.002	-0.492	200	0.025	0.014	-0.003	0.003	0.038
25	-0.827	-0.029	0.002	-0.005	-0.858	300	-0.018	0.018	-0.006	0.003	-0.003
50	-0.902	-0.053	0.005	-0.009	-0.960				$^3F_3$		
100	-0.786	-0.078	0.008	-0.012	-0.869	10	0.009	0.000	0.000	0.000	0.009
150	-0.685	-0.091	0.009	-0.011	-0.778	25	0.044	0.000	0.000	0.000	0.044
200	-0.618	-0.101	0.011	-0.009	-0.717	50	0.093	0.000	0.000	0.000	0.093
300	-0.540	-0.118	0.012	-0.002	-0.648	100	0.141	0.001	0.000	0.000	0.142
			$^3P_1$			150	0.159	0.003	0.000	0.000	0.163
1	0.017	0.000	0.000	0.000	0.017	200	0.166	0.005	0.000	0.001	0.171
5	0.116	0.001	0.000	0.000	0.117	300	0.165	0.010	-0.001	0.002	0.177
10	0.203	0.002	0.000	0.001	0.206				$^1G_4$		
25	0.313	0.007	-0.001	0.003	0.322	25	-0.009	0.000	0.000	0.000	-0.009
50	0.346	0.016	-0.004	0.008	0.366	50	-0.023	0.000	0.000	0.000	-0.023
100	0.323	0.032	-0.009	0.018	0.364	100	-0.032	0.001	0.000	0.000	-0.032
150	0.289	0.046	-0.014	0.028	0.349	150	-0.029	0.002	0.000	0.000	-0.027
200	0.259	0.058	-0.020	0.037	0.335	200	-0.022	0.003	0.000	0.000	-0.019
300	0.213	0.083	-0.032	0.057	0.321	300	-0.005	0.006	0.000	0.000	0.001
			$^1D_2$						$^3F_4$		
5	-0.009	0.000	0.000	0.000	-0.009	25	-0.004	0.000	0.000	0.000	-0.004
10	-0.025	0.000	0.000	0.000	-0.025	50	-0.015	0.000	0.000	0.000	-0.015
25	-0.052	0.001	0.000	0.000	-0.050	100	-0.037	0.000	0.000	0.000	-0.037
50	-0.045	0.005	0.000	0.000	-0.040	150	-0.053	0.000	0.000	0.000	-0.053
100	0.003	0.015	-0.001	0.001	0.018	200	-0.064	0.000	0.000	-0.001	-0.065
150	0.044	0.025	-0.001	0.001	0.069	300	-0.078	-0.001	0.000	-0.001	-0.080
200	0.071	0.034	-0.002	0.002	0.106				$^3H_4$		
300	0.100	0.047	-0.002	0.002	0.147	50	-0.007	0.000	0.000	0.000	-0.007
			$^3P_2$			100	-0.019	0.000	0.000	0.000	-0.019
5	-0.010	0.000	0.000	0.000	-0.011	150	-0.028	0.000	0.000	0.000	-0.029
10	-0.030	0.000	0.000	-0.001	-0.032	200	-0.035	0.000	0.000	0.000	-0.036
25	-0.096	-0.001	-0.001	-0.003	-0.101	300	-0.044	-0.001	0.000	0.000	-0.045
50	-0.172	-0.003	-0.002	-0.007	-0.184				$\epsilon_4$		
100	-0.224	-0.007	-0.005	-0.014	-0.250	25	0.012	0.000	0.000	0.000	0.012
150	-0.224	-0.007	-0.007	-0.019	-0.258	50	0.033	0.000	0.000	0.000	0.033
200	-0.210	-0.007	-0.008	-0.022	-0.248	100	0.058	0.000	0.000	0.000	0.059
300	-0.183	-0.004	-0.010	-0.022	-0.219	150	0.067	0.001	0.000	0.000	0.068
			$^3F_2$			200	0.068	0.001	0.000	0.000	0.070
10	-0.004	0.000	0.000	0.000	-0.004	300	0.062	0.002	0.000	0.000	0.065
25	-0.020	0.000	0.000	0.000	-0.020						

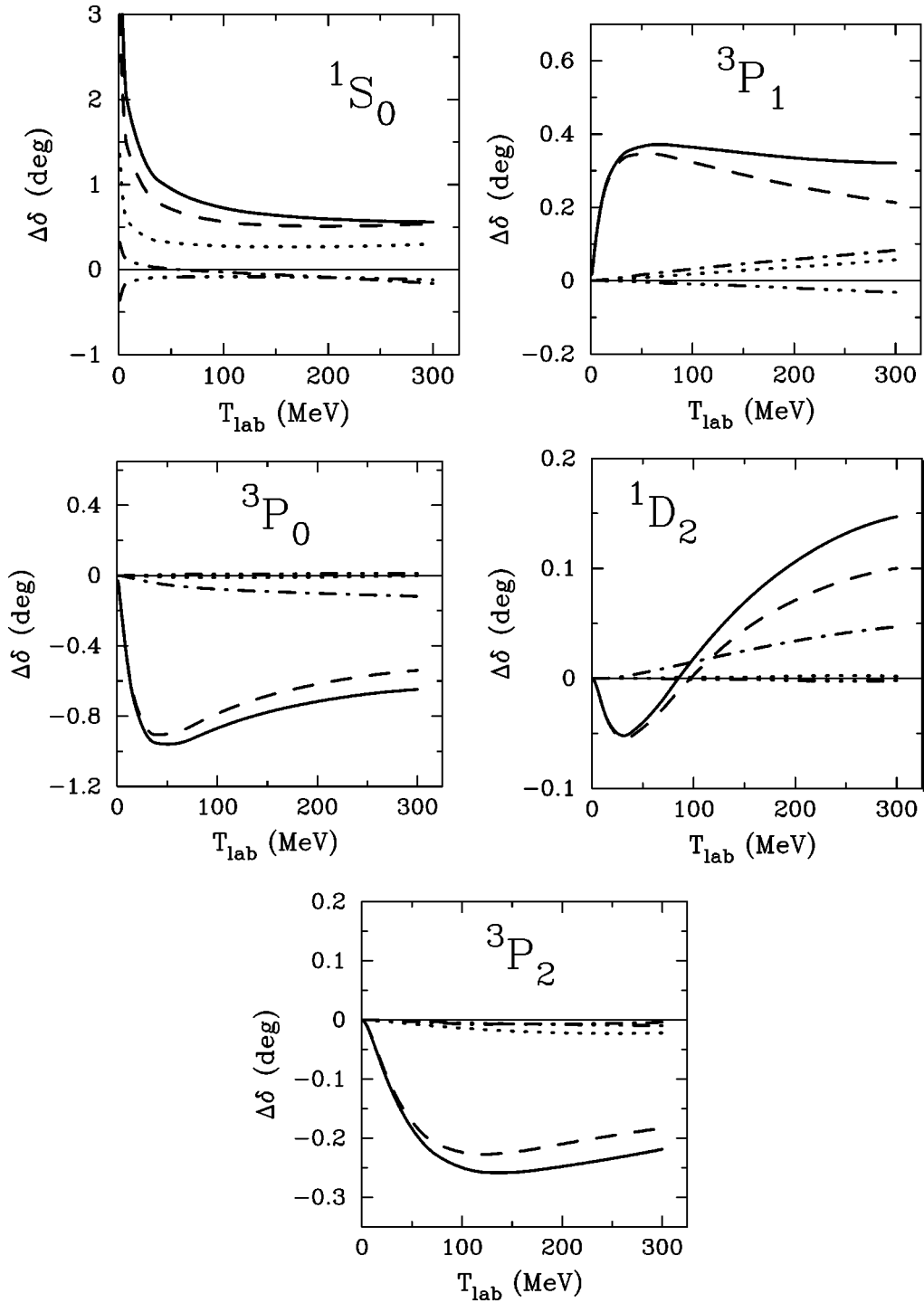


FIG. 5. CIB phase-shift differences  $\Delta\delta_{CIB}^{LSJ}$  (in degrees) as defined in Eq. (9) for laboratory kinetic energies  $T_{lab}$  below 300 MeV and partial waves with total angular momentum  $J \leq 2$ . The CIB effects due to OPE, the entire  $2\pi$  model,  $\pi\rho$  exchanges, and  $(\pi\sigma + \pi\omega)$  contributions are shown by the dashed, dash-dot, dash-triple-dot, and dotted curves, respectively. The solid curve is the sum of all CIB effects. (See text for further explanations.)

(stretched) box effect, in most partial waves. The total CIB effect from all diagrams of Fig. 2 is displayed by the dashed curve in Fig. 6.

(3)  $2\pi$  exchange with  $N\Delta$  intermediate states ( $2\pi N\Delta$ ), Fig. 3: Notice again, that every box stands for all possible time orderings of the box type (diagrams 1–6 of Fig. 20 of Ref. [8]) and every crossed box for all possible timeorderings of the crossed box type (diagrams 7 to 12 of Fig. 20 of Ref.

[8]). Thus, the total number of diagrams which Fig. 3(a) stands for is 24, while Fig. 3(b) stands for 48 diagrams, which are all explicitly taken into account in our calculations. Replacement of the boxes Fig. 3(a) by the boxes Fig. 3(b) causes an increase in the strength of these diagrams which, since these are attractive diagrams, causes an increase in attraction. Column  $2\pi N\Delta - B$  in Table II clearly confirms this. For the crossed boxes one gets typically the opposite

TABLE II. CIB phase-shift differences (in degrees) as defined in Eq. (9) for the various  $2\pi$ -exchange contributions explained in the text.  $S$  denotes stretched-box diagrams,  $B$  denotes box, and  $X$  denotes crossed-box diagrams.

$T_{\text{lab}}$ (MeV)	$2\pi NN-S$	$2\pi NN-X$	$2\pi N\Delta-B$	$2\pi N\Delta-X$	$2\pi\Delta\Delta-B$	$2\pi\Delta\Delta-X$	Total $2\pi$
$^1S_0$							
1	-0.182	0.319	0.692	-0.410	-0.244	0.143	0.319
5	-0.098	0.160	0.363	-0.217	-0.130	0.076	0.154
10	-0.075	0.113	0.271	-0.165	-0.099	0.058	0.103
25	-0.056	0.065	0.188	-0.119	-0.072	0.042	0.047
50	-0.047	0.037	0.146	-0.099	-0.061	0.034	0.009
100	-0.045	0.012	0.118	-0.091	-0.056	0.030	-0.031
150	-0.047	-0.003	0.109	-0.093	-0.058	0.030	-0.061
200	-0.052	-0.015	0.107	-0.100	-0.062	0.031	-0.091
300	-0.067	-0.041	0.112	-0.126	-0.078	0.037	-0.163
$^3P_0$							
10	-0.003	-0.003	0.001	-0.003	0.000	0.000	-0.009
25	-0.010	-0.010	0.002	-0.009	-0.001	0.000	-0.029
50	-0.018	-0.020	0.002	-0.017	-0.002	0.000	-0.053
100	-0.025	-0.030	0.003	-0.024	-0.002	0.001	-0.078
150	-0.027	-0.036	0.002	-0.028	-0.003	0.001	-0.091
200	-0.029	-0.041	0.002	-0.030	-0.003	0.001	-0.101
300	-0.031	-0.050	0.000	-0.035	-0.004	0.001	-0.118
$^3P_1$							
10	0.000	0.002	0.001	-0.001	0.000	0.000	0.002
25	-0.001	0.006	0.004	-0.002	0.000	0.000	0.007
50	-0.002	0.012	0.010	-0.003	-0.001	0.001	0.016
100	-0.003	0.021	0.021	-0.006	-0.001	0.001	0.032
150	-0.004	0.028	0.030	-0.008	-0.002	0.002	0.046
200	-0.004	0.034	0.038	-0.009	-0.002	0.002	0.058
300	-0.004	0.043	0.054	-0.010	-0.003	0.003	0.083
$^1D_2$							
50	0.000	0.003	0.002	0.000	0.000	0.000	0.005
100	0.000	0.009	0.007	-0.001	0.000	0.000	0.015
150	0.000	0.014	0.013	-0.002	-0.001	0.001	0.025
200	0.000	0.017	0.019	-0.003	-0.001	0.001	0.034
300	0.000	0.020	0.031	-0.004	-0.002	0.002	0.047
$^3P_2$							
10	-0.001	0.001	0.001	-0.001	0.000	0.000	0.000
25	-0.003	0.002	0.005	-0.004	-0.001	0.001	-0.001
50	-0.006	0.004	0.011	-0.010	-0.004	0.002	-0.003
100	-0.009	0.004	0.020	-0.018	-0.008	0.004	-0.007
150	-0.010	0.004	0.027	-0.022	-0.011	0.005	-0.007
200	-0.010	0.003	0.031	-0.024	-0.014	0.007	-0.007
300	-0.009	0.003	0.037	-0.024	-0.018	0.008	-0.004

effect (column  $2\pi N\Delta-X$  of Table II). This partial cancellation of the effects from the two groups of diagrams is also demonstrated in Fig. 6 where the dash-dot curve represents the effect from the box diagrams while the dash-triple-dot curve is from the crossed ones. Notice that the cancellation is almost perfect in  $^1S_0$  and  $^3P_2$  even though the individual contributions are rather large.

(4)  $2\pi$  exchange with  $\Delta\Delta$  intermediate states ( $2\pi\Delta\Delta$ ), Fig. 4: The replacement of the diagrams of Fig. 4(a) by Fig. 4(b) shows the by now familiar characteristic: opposite effects from box and crossed box diagrams (column  $2\pi\Delta\Delta-B$  and  $2\pi\Delta\Delta-X$  of Table II). This results in large cancellations between effects which, due to the short-range nature of this class of diagrams, are individually already rather

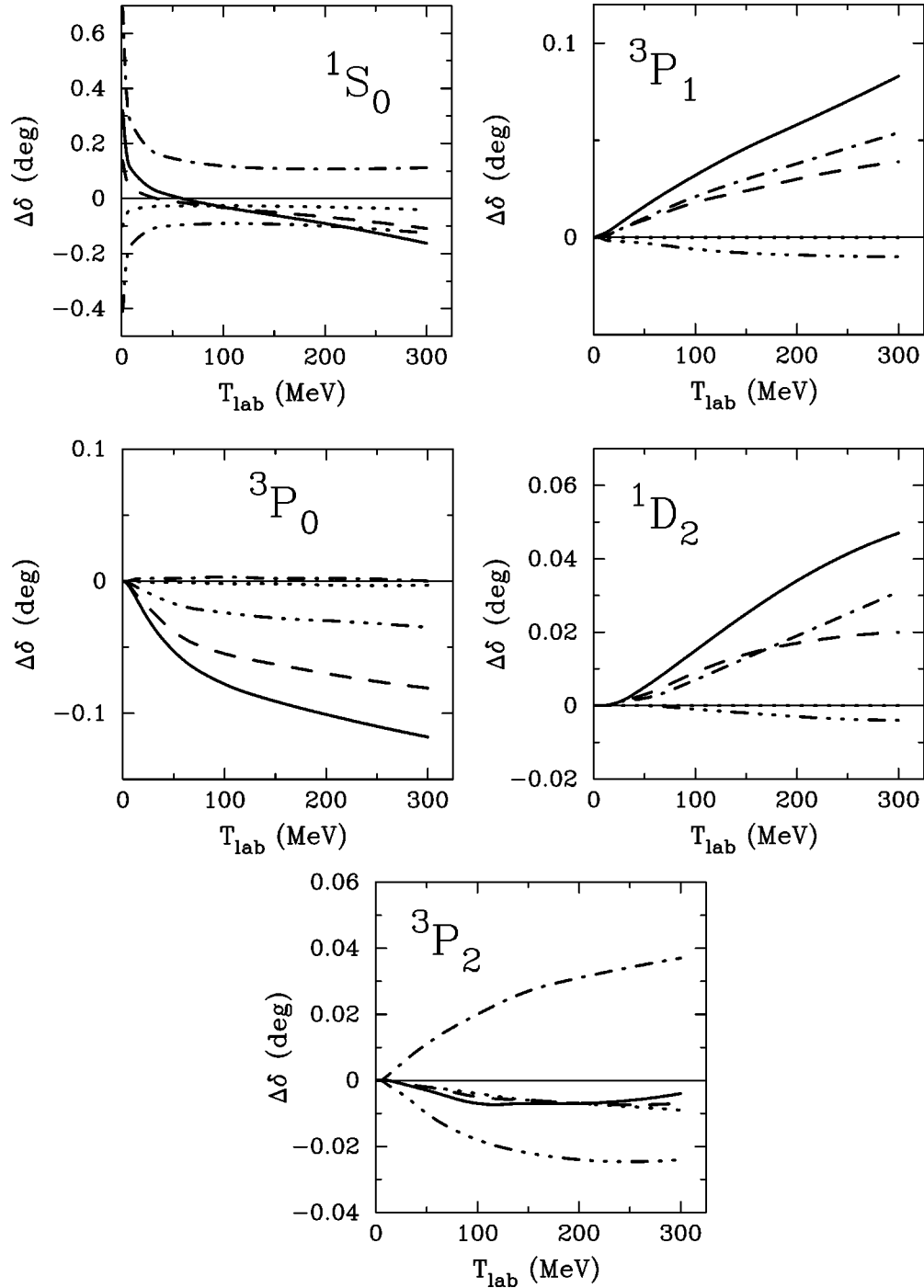


FIG. 6. Similar to Fig. 5, but here the individual contributions from the  $2\pi$  model are shown. The CIB effects due to  $2\pi NN$ ,  $2\pi N\Delta$ - $B$ ,  $2\pi N\Delta$ - $X$ , and  $2\pi\Delta\Delta$  are shown by the dashed, dash-dot, dash-triple-dot, and dotted curves, respectively. The solid curve is the sum of all CIB effects due to the exchange of two pions. (See text and caption of Table II for further explanations.)

small. This explains why the CIB effect from the diagrams of Fig. 4 is negligible in most partial waves (dotted curve in Fig. 6).

This finishes the discussion of all contributions of the  $2\pi$  type. In summary, one can say that the total CIB effect from  $2\pi$  (dash-dot curve in Fig. 5) is quite noticeable up to the  $D$  state. In  $^1S_0$ ,  $^3P_0$ ,  $^3P_1$ , and  $^1D_2$ , the CIB effect from  $2\pi$  is 20–50% of the one from OPE, at 300 MeV. However, for low energies (except in  $^1S_0$ ) as well as in higher partial waves, the CIB  $2\pi$  effect is negligible.

(5)  $\pi\rho$  exchanges. This group is, in principal, as compre-

hensive as the  $2\pi$  exchanges discussed above. Graphically, the  $\pi\rho$  diagrams can be obtained by replacing in each diagram of Figs. 2–4, one of the two pions by a  $\rho$  meson of the same charge-state (because of this simple analogy, we do not show the  $\pi\rho$  diagrams explicitly here). Concerning the  $\pi\rho$  diagrams with  $\Delta$  intermediate states a comment is in place. In the Bonn model [8], the crossed  $\pi\rho$  diagrams with  $N\Delta$  and  $\Delta\Delta$  intermediate states are included in terms of an approximation. It is assumed that they differ from the corresponding box diagrams only by the isospin factor. Thus, the  $\pi\rho$  box diagrams with  $N\Delta$  and  $\Delta\Delta$  intermediate states are

TABLE III. CIB contributions to the  $^1S_0$  scattering length,  $\Delta a_{\text{CIB}}$ , and effective range,  $\Delta r_{\text{CIB}}$ , from various components of the  $NN$  interaction as explained in the text.

	OPE	$2\pi$	$\pi\rho$	$\pi\sigma + \pi\omega$	Total	Empirical
$\Delta a_{\text{CIB}}$ (fm)	3.243	0.360	-0.383	1.426	4.646	$5.7 \pm 0.5$
$\Delta r_{\text{CIB}}$ (fm)	0.099	0.002	-0.006	0.020	0.115	$0.05 \pm 0.13$

multiplied by an isospin factor that is equal to the sum of the isospin factors for box and crossed box. In this approximation, these diagrams do not generate any CIB effects due to pion-mass splitting. Since these diagrams are of very short range, their CIB effect may be negligible, anyhow. The only class of  $\pi\rho$  diagrams which we include in our calculation of CIB effects is the one that corresponds to Fig. 2, with one pion in each diagram replaced by a  $\rho$  meson. Its contribution to CIB (column  $\pi\rho$  of Table I and dash-triple-dot curve of Fig. 5) is generally small, and typically opposite to the one from  $2\pi$ , in most states.

(6) Further  $3\pi$  and  $4\pi$  contributions ( $\pi\sigma + \pi\omega$ ). The Bonn potential also includes some  $3\pi$  exchanges that can be approximated in terms of  $\pi\sigma$  diagrams and  $4\pi$  exchanges of the  $\pi\omega$  type. It was found in Ref. [8] that the sum of these contributions is small. These diagrams have  $NN$  intermediate states—similar to Fig. 2, but with one of the two exchanged pions replaced by an isospin-zero boson; thus, the isospin factors are different from the ones of Fig. 2 and, in fact, like the ones of Fig. 1. Another way of creating these diagrams is to combine the diagrams of Fig. 1 with a  $\sigma$  or an  $\omega$  in an irreducible way, i.e., by forming a stretched box or crossed box diagram. These diagrams carry the same isospin factors as OPE. Since this class of diagrams is part of the Bonn model, we include these diagrams in our CIB consideration. The CIB effect from this class is very small, except in  $^1S_0$ ,  $^3P_1$ , and  $^3P_2$  (Column  $\pi\sigma + \pi\omega$  of Table I and dotted curve in Fig. 5). This effect has always the same sign as the effect from OPE, but it is substantially smaller. The reason for the OPE character of this contribution is that  $\pi\sigma$  prevails over  $\pi\omega$  and, thus, determines the character of this contribution. Since  $\sigma$  exchange is negative and since, furthermore, the propagator in between the  $\pi$  and the  $\sigma$  exchange is also negative, the overall sign of the  $\pi\sigma$  exchange is the same as OPE. Thus, it is like a weak, short-ranged OPE.

This finishes our detailed presentation of the diagrams and their CIB effects included in our calculation. The sum of all CIB effects on phase shifts is given in the last column of Table I and plotted by the solid curve in Fig. 5. Notice that the difference between the solid curve and the dashed curve (OPE) in Fig. 5 represents the sum of all effects beyond OPE. Thus, it is clearly seen that OPE dominates the CIB

effect in all partial waves, even though there are substantial contributions besides OPE in some states, notably  $^1S_0$ ,  $^3P_1$ , and  $^1D_2$ .

Finally, in Tables III and IV, we also give the CIB contributions to the  $^1S_0$  scattering length and effective range. Note that the relationship between the CIB potential and the corresponding change of the scattering length,  $\Delta a_{\text{CIB}}$ , is highly nonlinear. As discussed in Refs. [5,3], when the scattering length changes from  $a_1$  to  $a_2$  due to a CIB potential  $\Delta V = V_1 - V_2$ , the relationship is

$$\frac{1}{a_2} - \frac{1}{a_1} = M_N \int_0^\infty \Delta V u_1 u_2 dr \quad (11)$$

or

$$a_1 - a_2 = a_1 a_2 M_N \int_0^\infty \Delta V u_1 u_2 dr, \quad (12)$$

with  $u_1$  and  $u_2$  the zero-energy  $^1S_0$  wave functions normalized such that  $u(r \rightarrow \infty) \rightarrow (1 - r/a)$ . Thus, the perturbation expansion concerns the inverse scattering length. As clearly evident from Eq. (12), the change of the scattering length depends on the ‘‘starting value’’  $a_1$  to which the effect is added. In our calculations, CIB effects are generated step by step, which implies that the starting value  $a_1$  is different for each CIB effect. This distorts the relative size of different CIB contributions to the scattering length difference. To make the relative comparison meaningful, we have rescaled our results for  $\Delta a_{\text{CIB}}$  according to a prescription given by Ericson and Miller [5], which goes as follows. Assume the ‘‘starting value’’ for the scattering length is  $a_1$  and a certain CIB effect brings it up to  $a_2$ . Then, the resulting scattering length difference ( $a_1 - a_2$ ) is rescaled by

$$\Delta a = (a_1 - a_2) \frac{\bar{a} a_{np}}{a_1 a_2} \quad (13)$$

with  $\bar{a} = -18.05$  fm and  $a_{np} = -23.75$  fm. This will make  $\Delta a$  independent of the choice for  $a_1$ . The numbers given in Table III and IV for  $\Delta a_{\text{CIB}}$  are all rescaled according to Eq. (13).

We obtain a total  $\Delta a_{\text{CIB}}$  of 4.65 fm which is about 80% of the empirical value of 5.7 fm [Eq. (4)]. For  $\Delta r_{\text{CIB}}$  we find a total of 0.115 fm from all effects, consistent with the empirical value [Eq. (5)]. Even though our total result for  $\Delta a_{\text{CIB}}$  is very similar to the earlier calculation of Ref. [3], there are some differences in the details. For the total effect from  $2\pi$  exchange we obtain in the present calculations  $\Delta a_{\text{CIB}} = 0.36$  fm while in Ref. [3] 0.85 fm was reported. This is due to differences in the interpretation of the scaling mass that oc-

TABLE IV. CIB contributions to the  $^1S_0$  scattering length,  $\Delta a_{\text{CIB}}$ , and effective range,  $\Delta r_{\text{CIB}}$ , for the various parts of the  $2\pi$ -exchange model as explained in the text.  $S$  denotes stretched-box diagrams,  $B$  denotes box, and  $X$  denotes crossed-box diagrams.

	$2\pi NN-S$	$2\pi NN-X$	$2\pi N\Delta-B$	$2\pi N\Delta-X$	$2\pi\Delta\Delta-B$	$2\pi\Delta\Delta-X$	Total $2\pi$
$\Delta a_{\text{CIB}}$ (fm)	-0.196	0.351	0.787	-0.470	-0.272	0.159	0.360
$\Delta r_{\text{CIB}}$ (fm)	-0.003	0.003	0.010	-0.006	-0.004	0.002	0.002

curs in the  $N\Delta\pi$  Lagrangian, Eq. (8). While in the present calculations we always use  $m_{\pi^\pm}$  [see discussion below Eq. (8)], in the earlier calculations of Ref. [3]  $m_{\pi^0}$  was used for  $\pi^0$  coupling and  $m_{\pi^\pm}$  for  $\pi^\pm$  coupling. The latter convention introduces a strong charge dependence of the effective  $N\Delta\pi$  coupling strength, which enhances the CIB effects from all diagrams involving  $\Delta$  isobars. In principal, there is discretion in how to deal with the scaling mass in Eq. (8). However, in the present calculations, we decided to follow the established convention [12]. As a result, the effect from  $2\pi$  exchange is smaller than in the earlier calculation of Ref. [3].

There is also a small difference in the  $\Delta a_{\text{CIB}}$  contribution from noniterative  $\pi\sigma$  and  $\pi\omega$  exchanges for which we obtain 1.4 fm, while Ref. [3] reported 1.2 fm. This discrepancy is due to the fact that in Ref. [3] a preliminary version of the Bonn Full Model [4] was used, while here we applied the final version [8] in which the strength of the  $\pi\sigma$  contribution is slightly larger, which explains the difference.

We note that the CIB effect depends on the  $\pi NN$  coupling constant. In the present calculations, we follow the Bonn model [8]: we assume charge independence of the coupling constant and use  $g_\pi^2/4\pi = 14.4$  [13]. In recent years, there has been some controversy about the precise value of the  $\pi NN$  coupling constant. Unfortunately, the problem is far from being settled. Based upon  $NN$  phase-shift analysis, the Nijmegen group [14] advocates the ‘‘small’’ charge-independent value  $g_\pi^2/4\pi = 13.5(1)$ , while a very recent determination by the Uppsala group [15] based upon high precision  $np$  charge-exchange data at 162 MeV resulted in the ‘‘large’’ value  $g_\pi^2/4\pi = 14.52(26)$ . Other recent determinations are in-between the two extremes: The VPI group [16] quotes  $g_\pi^2/4\pi = 13.77(15)$  from  $\pi N$  and  $NN$  analysis with no evidence for charge dependence. Bugg and Machleidt [17] obtain  $g_\pi^2/4\pi = 13.69(39)$  and  $g_\pi^2/4\pi = 13.94(24)$  from the analysis of  $NN$  elastic data between 210 and 800 MeV. Because of this large uncertainty in the  $\pi NN$  coupling constant, it might be of interest to know what the CIB effects are like when a value is used that deviates substantially from our choice. For that reason, we have repeated our CIB calculations with the smaller values  $g_\pi^2/4\pi = 14.0$  and  $13.6$ . It turns out that the total CIB effect on phase shifts (last column of Table I) as well as the effect on the effective range parameters (Table III) scales linearly with the  $\pi NN$  coupling constant, to a good approximation. To be precise: multiplying the total phase-shift differences in Table I or the effective range changes in Table III with  $13.6/14.4$  reproduces within  $\pm 2\%$  the exact results from a CIB calculation that employs  $g_\pi^2/4\pi = 13.6$ .

As last item in our study, we have also investigated the effect of  $\rho$ -mass splitting on the  $^1S_0$  effective range parameters. Unfortunately, the evidence for  $\rho$ -mass splitting is very uncertain, with the Particle Data Group [11] reporting  $m_{\rho^0} - m_{\rho^\pm} = 0.3 \pm 2.2$  MeV. Consistent with this, we assumed in our exploratory study  $m_{\rho^0} = 769$  MeV and  $m_{\rho^\pm} = 768$  MeV, i.e., a splitting of 1 MeV. With this, we find  $\Delta a_{\text{CIB}} = -0.29$  fm from one- $\rho$ -exchange, and  $\Delta a_{\text{CIB}} = 0.28$  fm from the noniterative  $\pi\rho$  diagrams with  $NN$  intermediate states. Thus, individual effects are small and, in addition, there are substantial cancellations between the two classes of diagrams that contribute. The net result is a vanishing effect. Thus,

even if the  $\rho$ -mass splitting will be better determined in the future and may turn out to be larger than our assumption, it will never be a great source of CIB.

### III. SUMMARY AND CONCLUSIONS

Based upon the Bonn meson-exchange model for the  $NN$  interaction, we have calculated the CIB effects due to pion-mass splitting on the singlet effective range parameters and on the phase shifts of  $NN$  scattering for partial waves of total angular momentum  $J \leq 4$  and laboratory energies below 300 MeV. This investigation complements our recent paper on charge-asymmetry of the  $NN$  interaction [7].

The overall results may be characterized as follows.

The largest phase-shift differences occur in the  $^1S_0$  state where they are most noticeable at low energy; e.g., at 1 MeV, the difference is  $4.36^\circ$ , indicating that the  $np$  nuclear force is more attractive than the  $pp$  nuclear force. The  $^1S_0$  phase-shift difference decreases with increasing energy and is about  $0.6^\circ$  at 300 MeV. The major part of the phase-shift difference comes from OPE. CIB contributions from two-meson exchange diagrams can be large, but there are typically cancellations between the effects from different classes of diagrams of the two-meson type.

The CIB effect on the phase shifts of  $P$  and higher partial waves is generally small. The most significant difference is found in the  $^3P_0$  state around 50 MeV where the difference is almost 1 degree. In  $P$  waves, the difference is roughly constant above 25 MeV: it is  $0.95 - 0.65^\circ$  in  $^3P_0$ , about  $0.35^\circ$  in  $^3P_1$ , and around  $0.2^\circ$  in  $^3P_2$ . In all other partial waves, it is in the order of  $0.1^\circ$  or less. Again, the main effect comes from OPE, however, in  $^3P_0$ ,  $^3P_1$ , and  $^1D_2$  at 300 MeV, the effect from the  $2\pi$  model is in the range of 20–50% of the one from OPE.

The fact that the magnitudes of the phase-shift differences in all partial waves, except  $^1S_0$ , are small, makes it difficult to verify experimentally the charge-dependent effects in  $P$  and higher partial waves. However, since the phase shifts in these states themselves are small, the relative magnitudes of the phase shift differences are not negligible and could have a noticeable effect on some sensitive observables such as the analyzing power ( $A_y$ ) in nucleon-deuteron ( $nd$ ) scattering [18] since this reaction blows up effects from triplet  $P$  waves [19]. Our microscopic predictions are, however, substantially smaller than what is needed to solve the  $nd$   $A_y$  puzzle [18,20].

As mentioned in the Introduction, another CIB contribution to the nuclear force is irreducible pion-photon ( $\pi\gamma$ ) exchange. Traditionally, it was believed that this contribution would take care of the remaining 20% of  $\Delta a_{\text{CIB}}$  [5,2]. However, a recently derived  $\pi\gamma$  potential based upon chiral perturbation theory [21] decreases  $\Delta a_{\text{CIB}}$  by about 0.6 fm, making the discrepancy even larger. Thus, we are faced with the fact that about 20–30% of the charge dependence of the singlet scattering length is not explained.

In recent years, nuclear physicists have become increasingly concerned with chiral symmetry which is an approximate symmetry of QCD in the light-quark sector. In the light of these new views, the  $NN$  interaction should have a clear relationship with chiral symmetry. The Bonn model that our investigation is based upon is, by construction, not a consis-

tently chiral model. Chiral models for the  $NN$  interaction and, in particular, chiral models for the  $2\pi$  exchange have recently been constructed by various groups [22–24]. However, most of these models are applicable only for the peripheral partial waves of  $NN$  scattering and not for  $S$ ,  $P$ , or  $D$  waves; and if there are predictions for lower partial waves, they are only of qualitative nature. The CIB effects in  $S$  and  $P$  waves and, particularly, for the singlet scattering length are very subtle and, therefore, require a quantitative model. Thus, current chiral models for the  $2\pi$  exchange are not (yet) suitable for reliable calculations of CIB. One may then raise an interesting question: What has to be changed in the Bonn model to make it chiral? This question can be answered precisely. The diagrams in Figs. 2(a) and 2(b) of Ref. [22] have to be added to the Bonn model; that is essentially all. These diagrams include the Weinberg-Tomozawa  $\pi\pi NN$  vertex which is a characteristic ingredient of any nonlinear realization of chiral symmetry. However, it has been found independently by different groups [22–24] that the  $2\pi$  exchange diagrams which include the Weinberg-Tomozawa vertex make a very small, essentially negligible,

contribution to the  $NN$  interaction. One may then expect that the CIB caused by these diagrams is also very small [25]. Thus, there are reasons to believe that the results of this study may be of broader relevance than what the (formally) nonchiral character of our model suggests. Of course, the final and reliable answer of the question under consideration can only come from a “perfect” and quantitative chiral model for the  $NN$  interaction that is applicable also in  $S$  waves and for the calculation of scattering lengths. In view of the problems raised concerning scattering length calculations with chiral models [26,27] and in view of the continuing general controversy concerning cutoff *versus* dimensional regularization, it will take many years until a reliable calculation of this kind can be done. Thus, for the time being, it may be comforting to have at least our present results.

#### ACKNOWLEDGMENTS

This work was supported in part by the U.S. National Science Foundation under Grant No. PHY-9603097 and by the Idaho State Board of Education.

- 
- [1] G. A. Miller, B. M. K. Nefkens, and I. Slaus, *Phys. Rep.* **194**, 1 (1990).
- [2] G. A. Miller and W. H. T. van Oers, in *Symmetries and Fundamental Interactions in Nuclei*, edited by W. C. Haxton and E. M. Henley (World Scientific, Singapore, 1995) p. 127.
- [3] C. Y. Cheung and R. Machleidt, *Phys. Rev. C* **34**, 1181 (1986).
- [4] R. Machleidt, in *Quarks and Nuclear Structure*, Proceedings of the Third Klaus Erkelenz Symposium, Bad Honnef, 1983, Lecture Notes in Physics, Vol. 197, edited by K. Bleuler (Springer, Heidelberg, 1984), p. 352.
- [5] T. E. O. Ericson and G. A. Miller, *Phys. Lett.* **132B**, 32 (1983).
- [6] M. H. Partovi and E. L. Lomon, *Phys. Rev. D* **2**, 1999 (1970).
- [7] G. Q. Li and R. Machleidt, *Phys. Rev. C* **58**, 1393 (1998).
- [8] R. Machleidt, K. Holinde, and Ch. Elster, *Phys. Rep.* **149**, 1 (1987).
- [9] R. Machleidt, *Adv. Nucl. Phys.* **19**, 189 (1989).
- [10] R. Machleidt and G. Q. Li, *Phys. Rep.* **242**, 5 (1994).
- [11] Particle Data Group, K. Hikasa *et al.*, *Phys. Rev. D* **45**, S1 (1992).
- [12] O. Dumbrajs *et al.*, *Nucl. Phys.* **B216**, 277 (1983).
- [13] The relationship between  $g_\pi$  and  $f_{\pi NN}$  [the latter being used in the Lagrangian Eq. (7)] is  $g_\pi^2 = (2M_N/m_{\pi^\pm})^2 f_{\pi NN}^2 = 181.027 f_{\pi NN}^2$ . Following the Bonn model [8], we also assume a fixed relationship between  $f_{\pi N\Delta}$  [used in the Lagrangian Eq. (8)] and  $f_{\pi NN}$ , namely,  $f_{\pi N\Delta}^2 = \frac{7}{25} f_{\pi NN}^2$ .
- [14] V. Stoks, R. Timmermans, and J. J. de Swart, *Phys. Rev. C* **47**, 512 (1993).
- [15] J. Rahm *et al.*, *Phys. Rev. C* **57**, 1077 (1998).
- [16] R. A. Arndt, R. L. Workman, and M. M. Pavan, *Phys. Rev. C* **49**, 2729 (1994); R. A. Arndt, I. I. Strakovsky, and R. L. Workman, *ibid.*, **52**, 2246 (1995).
- [17] D. V. Bugg and R. Machleidt, *Phys. Rev. C* **52**, 1203 (1995).
- [18] H. Witala and W. Glöckle, *Nucl. Phys.* **A528**, 48 (1991); W. Glöckle, H. Witala, D. Hüber, H. Kamada, and J. Golak, *Phys. Rep.* **274**, 107 (1996).
- [19] I. Slaus, R. Machleidt, W. Tornow, W. Glöckle, and W. Witala, *Comments Nucl. Part. Phys.* **20**, 85 (1991).
- [20] D. Hueber and J. L. Friar, *Phys. Rev. C* **58**, 674 (1998).
- [21] U. van Kolck, M. C. M. Rentmeester, J. L. Friar, T. Goldman, and J. J. de Swart, *Phys. Rev. Lett.* **80**, 4386 (1998).
- [22] C. Ordóñez, L. Ray, and U. van Kolck, *Phys. Rev. C* **53**, 2086 (1996).
- [23] M. R. Robilotta and C. A. da Rocha, *Nucl. Phys.* **A615**, 391 (1997).
- [24] N. Kaiser, R. Brockmann, and W. Weise, *Nucl. Phys.* **A625**, 758 (1997).
- [25] U. van Kolck (private communication).
- [26] K. A. Scaldeferri, D. R. Philipps, C. W. Kao, and T. D. Cohen, *Phys. Rev. C* **56**, 679 (1997).
- [27] D. B. Kaplan, M. B. Savage, and M. B. Wise, *Nucl. Phys.* **B478**, 629 (1996).